

Earthquake relocation in the Central Alborz region of Iran using a non-linear probabilistic method

Vahid Maleki · Z. Hossein Shomali ·
Mohammad Reza Hatami · Mehrdad Pakzad ·
Anthony Lomax

Received: 23 March 2012 / Accepted: 25 October 2012 / Published online: 18 January 2013
© Springer Science+Business Media Dordrecht 2013

Abstract In this study, we calculate accurate absolute locations for nearly 3,000 shallow earthquakes (≤ 20 km depth) that occurred from 1996 to 2010 in the Central Alborz region of northern Iran using a non-linear probabilistic relocation algorithm on a local scale. We aim to produce a consistent dataset with a realistic assessment of location errors using probabilistic hypocenter probability density functions. Our results indicate significant improvement in hypocenter locations and far less scattering than in the routine earthquake catalog. According to our results, 816 earthquakes have horizontal uncertainties in the 0.5–3.0 km range, and 981 earthquakes are relocated with focal-depth errors less than 3.0 km, even with a sub-optimal network geometry. Earthquake relocated are tightly clustered in the eastern Tehran region and are mainly associated with active faults in the study area (the Mosha and Garmsar faults). Strong historical earthquakes have occurred along the Mosha and Garmsar faults, and the relocated earthquakes along

these faults show clear north-dipping structures and align along east–west lineations, consistent with the predominant trend of faults within the study region. After event relocation, all seismicity lies in the upper 20 km of the crust, and no deep seismicity (>20 km depth) has been observed. In many circumstances, the seismicity at depth does not correlate with surface faulting, suggesting that the faulting at depth does not directly offset overlying sediments.

Keywords Earthquake relocation · Probability density functions · Non-linear probabilistic relocation algorithm · Seismicity

1 Introduction

The Alborz mountain belt in northern Iran is an active region of complex crustal deformation located in the central Alpine–Himalayan orogenic system. The Alborz mountain belt is 100 km wide and 600 km long and trends east–west, with many summits between 3,600 and 4,800 m elevation. Its present-day tectonics is characterized by high-angle faults that are mainly parallel to the mountain range (Fig. 1), with Damavand, a 5,671-m-elevation Quaternary volcano, in the center of the belt. The Alborz mountain belt is separated from the South Caspian Basin to the north by south-dipping faults (the Khazar and the North Alborz reverse faults; see Fig. 1) and from the Central Iran microplate to the south by north-dipping faults (the

V. Maleki · Z. H. Shomali · M. R. Hatami · M. Pakzad
Institute of Geophysics, University of Tehran,
Tehran 14155-6466, Iran

Z. H. Shomali (✉)
Department of Earth Sciences, Uppsala University,
Uppsala 75236, Sweden
e-mail: Hossein.Shomali@geo.uu.se

A. Lomax
ALomax Scientific,
Mouans-Sartoux, France

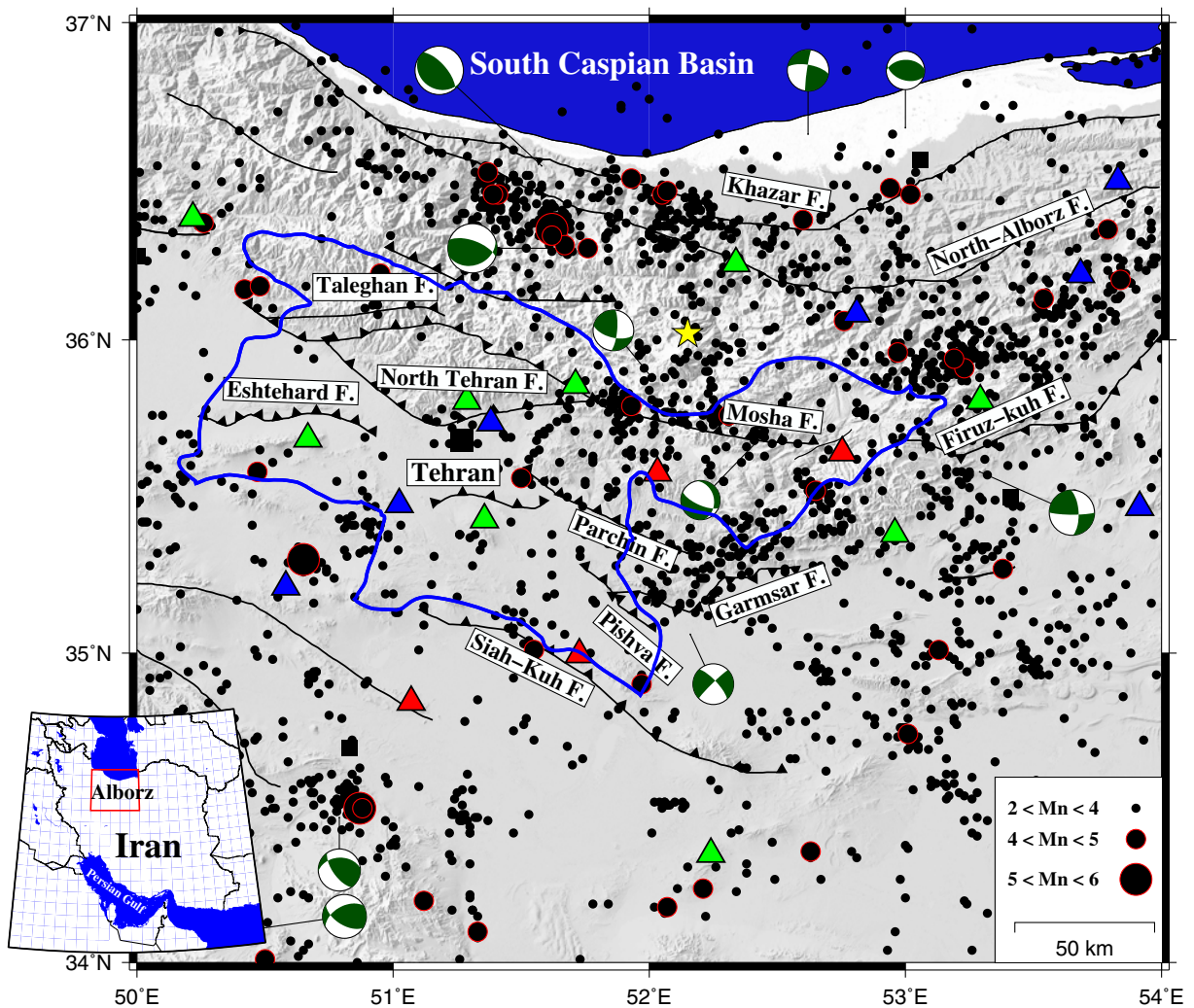


Fig. 1 IGUT catalog seismicity (*black circles*) for 1996–2010 and mapped faults (*black lines*) in the Central Alborz region. Only M_n 2.0–5.9 earthquakes that are recorded by more than six stations and have an RMS less than 1 s are shown (2,690 events). Seismic stations are colored according to their number of phases contributed to the inversion: *red* indicates 2,500–

5,000 phases; *green* indicates 1,000–2,500 phases, and *blue* indicates fewer than 1,000 phases. The Tehran province is marked by a *blue line*, and the main cities are denoted by *black squares*. The Damavand volcano is denoted by a *yellow star*. Fault plane solutions of large events ($M_w > 5.0$) are from the Global Centroid Moment Tensor Project catalog (2012)

Moshha and the North Tehran faults; see Fig. 1). The seismicity in the Central Alborz belt is distributed across the entire region and is quite shallow (<20 km depth) with dominant reverse or left-lateral strike-slip faults (Berberian 1976; Berberian and Yeats 1999; Ashtari et al. 2005). The region accommodates approximately 5 ± 2 mm/year of shortening and 4 ± 2 mm/year of left-lateral strike-slip motion (Vernant et al. 2004), with a total shortening of about 30 km near Tehran since the early Pliocene (Allen et al. 2003; Ashtari et al. 2005). Several strong historical earthquakes occurred in the

Central Alborz region with a return period of about 150 years (Ambraseys and Melville 1982; Moinfar et al. 1994), thus the assessed seismic hazard is significant in the capital city of Tehran, the main population center in the area. Historical seismicity suggests that the region has experienced earthquakes with magnitude $M_s \geq 7$, including the 1830 earthquake ($M_s \sim 7.1$) associated with the eastern part of the Moshha Fault and the fourth century BC earthquake ($M_s \sim 7.6$) related to the Garmsar Fault (Ambraseys and Melville 1982; Berberian and Yeats 1999; Berberian and Yeats 2001). The observed

seismicity (Fig. 1) is concentrated east of Tehran, where many clusters are observed that are associated with different active faults, e.g., the North Alborz Fault (a 150-km-long thrust fault), the Mosha Fault (a 180-km-long left-lateral strike-slip fault), and the Garmsar Fault (a 138-km-long thrust fault) (Berberian and Yeats 2001; see Fig. 1). The observed seismicity cluster might be associated with different patches of fault slip, but there are many places that the epicenter trends and patterns are not correlated with any known active faults. The main purpose of this study is to improve absolute earthquake locations for events recorded by the local seismic network in the Central Alborz region and to produce a consistent dataset with a realistic assessment of location errors using a non-linear probabilistic relocation technique. Comparison between the epicentral maps and hypocentral cross-sections is used to investigate whether the relocated hypocenter patterns delineate seismogenic structures or if they are artifacts caused by the ill-conditioned location problem. In this study, we conduct various synthetic tests and measures to assess the veracity of the hypocenter patterns produced by the relocation algorithm.

1.1 Nonlinear earthquake location

Earthquake hypocenter location is a non-linear process, and various iterative linearized algorithms have been widely implemented to determine hypocenter locations and their corresponding errors. Mainly due to increasing computer performance in the last decade, non-linear probabilistic earthquake location algorithms have repeatedly demonstrated their power as a tool for obtaining accurate earthquake locations (e.g., Tarantola and Valette 1982; Van Moser and Eck 1992; Lomax et al. 2000; Husen et al. 2003; Presti et al. 2004; Lomax 2005; Presti et al. 2008). In this study, we use the non-linear global-search probabilistic algorithm developed by Lomax et al. (2000), Lomax et al. (2001), and Lomax et al. (2009), known as NonLinLoc (NLL hereafter; www.alomax.net/nlloc), which has been applied in a number of prior studies, including Lomax (2005). In contrast to linearized methods where the hypocentral location of a single event is defined by a single point and its associated error, in NLL, the hypocenter location is determined by a set of points resulting from the posterior probability density function (PDF). The shape and the volume of PDF are proportional to the accuracy of the

hypocentral location and are consequently related to a number of factors, including phase-reading errors, the azimuthal gap, and network geometry. The shape of PDFs can be irregular and very different from the normal distribution assumed by linearized algorithms, and a compact PDF defines a well-constrained solution. In this study, the amount of data scatter is usually expressed as 68 % of the total population. An optimal hypocenter location is estimated in NLL by using the maximum likelihood (or minimum misfit) of the complete non-linear location of the PDF using an Oct-tree global search algorithm (see Lomax and Curtis 2001 and Lomax et al. 2009 for details). Theoretical travel times are calculated for a predefined 3D grid separately from the location procedure, providing an efficient way to incorporate a complex 3D velocity model in the location procedure. The NLL algorithm can also be applied using the equal differential-time (EDT) function (Font et al. 2004; Lomax 2005; Satriano et al. 2008). The objective function using EDT is defined based on the differences between the residuals for the observed and theoretical travel times of a single event recorded at a pair of stations. The EDT-PDF is independent of origin time and only depends on the latitude, longitude, and focal depth of an earthquake. EDT-PDF applications provide more reliable hypocenters in the presence of large outliers (e.g., Lomax 2005; Satriano et al. 2008; Lomax et al. 2009). The NLL algorithm also provides hypocentral uncertainties in different forms, including the error associated with latitude, longitude, and focal depth (ERX, ERY, and ERZ, respectively) and the uncertainty in the orientation and length of the principal axes of the error ellipsoid, as is done in HYPOELLIPSE (Lahr 1989); this error ellipsoid is determined by diagonalization of the covariance matrix using a singular value decomposition method (Lawson and Hanson 1974). Note that ERH and ERZ do not represent linearized measures; in other words, they are not calculated from a linearization of the solution at the optimal solution point but are determined from the PDFs as given below:

$$ERH = \sqrt{\text{cov}XX + \text{Cov}YY} \quad (1)$$

$$ERZ = \sqrt{\text{cov}ZZ} \quad (2)$$

where CovXX, CovYY, and CovZZ are diagonal

elements of the covariance matrix, respectively. Thus, a highly elongated and irregular PDF will have large error ellipsoid, ERH and ERZ. The NLL algorithm takes into account many factors that influence the quality of the hypocentral location process, such as errors in phase-reading, static station corrections, and the lack of a detailed velocity model. Previous studies have reported different location error estimates using linear and non-linear location algorithms (e.g., Lomax et al. 1998 using 1D velocity model; Satriano et al. 2008 using 3D velocity model). NLL provides travel-time weighting factors (parameter LOCGAU2) to represent variable uncertainties in the dataset as a function of travel times due to the effect of the station distribution and model error, similar to distance weighting used in many location algorithms (see the “Results” section for further explanation).

1.2 Earthquake dataset

The dataset used in this study contains earthquakes from 1996 through 2010 that occurred in the Central Alborz region (see Fig. 1) recorded by the Iranian Seismological Center (<http://irsc.ut.ac.ir/>) operated by the Institute of Geophysics, University of Tehran (IGUT). In the study area, the network consists of twenty three-component telemetered short-period sensors with average station spacing of 156 km. P-wave arrival times are routinely picked, and earthquakes locations are calculated using a single-event linearized location algorithm (the DAN-computer program developed by Nanometrics; e.g., Lee and Stewart 1981). Only earthquakes with a minimum of six arrival-time readings were selected from the IGUT earthquake catalog, resulting in a dataset that consists of 3,012 the Nuttli magnitude, M_n (Nuttli 1973) 2.0–6.3 earthquakes with 25,748 P-wave arrival times and 11,464 S-wave arrival times (Fig. 1). The study area, lying between latitude 50° – 54° E and longitude 34° – 37° N, was discretized using a 3D grid with a node spacing of $1 \times 1 \times 1$ km and $500 \times 500 \times 180$ cells along the x, y, and z axes, respectively. This grid was used both for forward travel-time calculation and for PDF calculations, and the grid spacing is related to station spacing and lateral velocity heterogeneity in the study volume. We used 1D starting velocity model developed by Ashtari et al. (2005) to calculate the theoretical travel times between each station and all grid nodes in the 3D volume prior to the location process.

Due to the lack of detailed information about the crustal velocity structure in the study area, Ashtari et al. (2005) searched for the best P-wave velocity structure model to fit the travel-time data using a 1D inversion procedure of the arrival times for micro-earthquakes recorded around the study area. They also estimated V_p/V_s by a least-square fit, keeping only travel-time data that are within twice the uncertainty.

2 Results

The relocated earthquakes in this study are shown in Fig. 2. We used the NLL location algorithm under the EDT constraint to obtain a solution that is less sensitive to outliers. In the dataset, these outliers are caused by various factors, including small SNR, signal-to-noise ratio, (especially for S-waves), bad phase readings or phase identification, suboptimal network conditions, and the lack of a reliable 3D velocity model of the complex crust in the region. Observational uncertainties for P- and S-phases of order of 0.01 and 0.05 s were assigned, respectively. In order to set reliable criteria to define well constraint locations, different synthetic tests were conducted to study the statistical information available in NLL results, including the difference between the maximum likelihood and the expected locations. Finally, the NLL location process was run for a predetermined set of travel-time weighting factors (parameter LOCGAU2) between 0.01 and 0.08. The final weighting factor assigned to each phase is inversely related to the product of the LOCGAU2 parameter and the travel time of the corresponding phase, limited to vary in the range of 0.2–3.0 s (parameter σ_T). The choice of LOCGAU2 and σ_T depend mainly on the precision of the forward solver used to compute synthetic travel times and the chosen grid spacing in the process. However, the expected precision of the forward solver and the error due to grid-spacing will and should be, in general, very small relative to the errors due to imperfect velocity structure. In contrast, not including approximate errors due to imperfect velocity structure may strongly de-stabilize and bias the location results, as these errors can be much larger than the picking errors. Effectively, not including these errors may introduce false outliers. These weighting factors ultimately assign lower weights to distant stations, similar to distance weighting used in many location algorithms, and

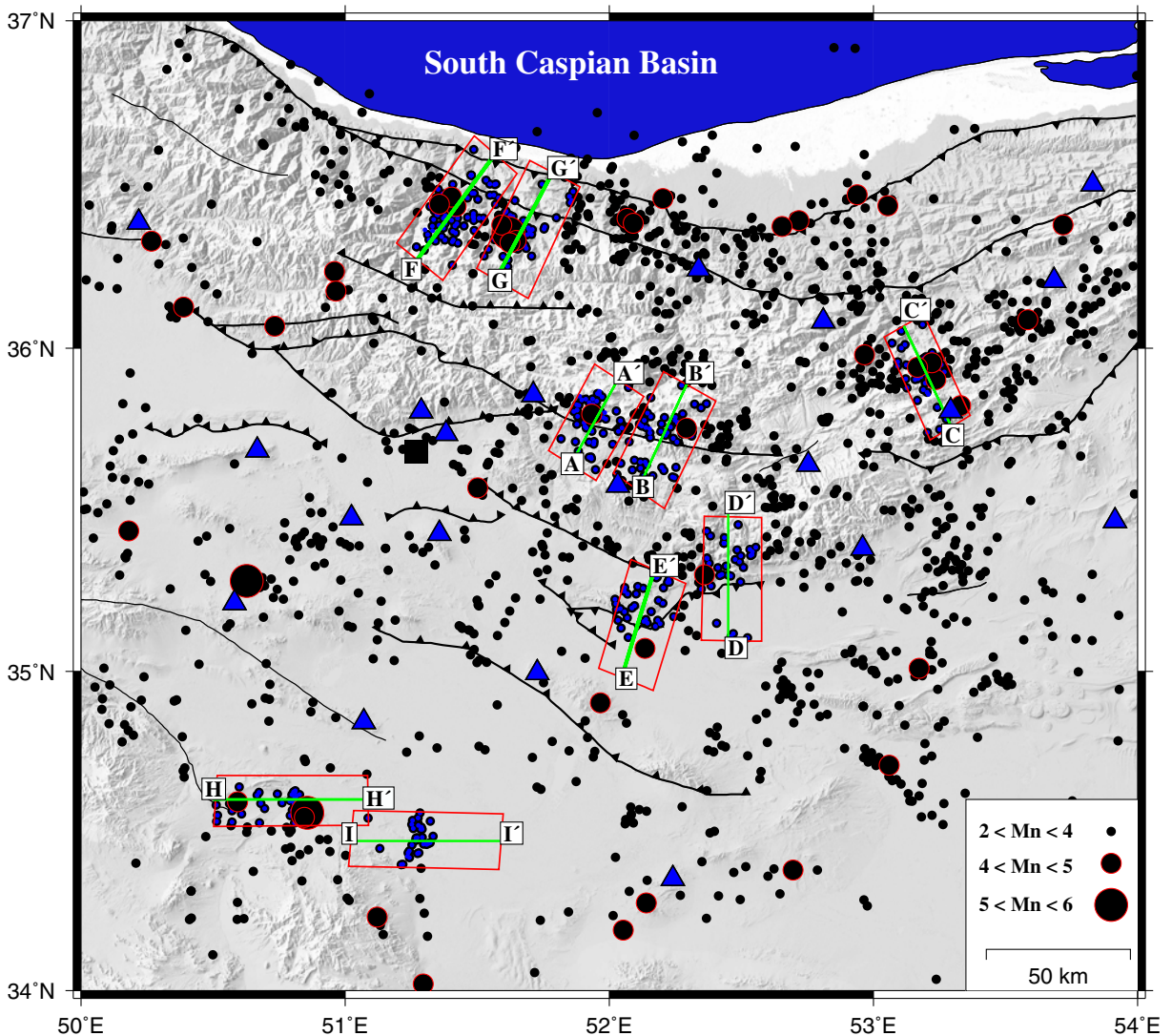


Fig. 2 A map of earthquakes relocated using the NLL algorithm. Only those solutions with horizontal errors less than 10 km and vertical errors less than 10 km are shown.

Earthquakes inside each *red rectangle* are plotted with the corresponding 68 % confidence ellipsoid in Fig. 5. Tectonic abbreviations are the same as in Fig. 1

are needed to stabilize the location algorithm, particularly in the presence of large outliers. Finally, the Oct-tree algorithm was used to further subdivide the cells with the highest probability values (e.g., Lomax and Curtis 2001; Lomax 2005; Satriano et al. 2008). For each earthquake, the solution with the smallest location error based on ERH and ERZ was selected as the optimal solution requiring that the difference between the maximum likelihood and expectation hypocenter locations to be small, e.g., less than 3.0 km for well-constrained solutions. The choice of, e.g., 3.0 km was based on the analysis of a large number of scatter PDF

plots indicating that in general events with a difference larger than 3.0 km had large uncertainties of several kilometers in epicenter and focal depth. An ill-conditioned location problem such as irregular location uncertainties with multiple minima can cause a large difference between the maximum likelihood and expectation hypocenter locations (Lomax et al. 2000; Husen and Smith 2004). Under such conditions, Gaussian location estimates, e.g., the confidence ellipsoid cannot be used to represent the location uncertainties (Husen and Smith 2004). In the relocated dataset, 816 events have horizontal uncertainties from 0.5–3.0 km, and 981 events

have focal-depth uncertainties less than 3.0 km (see Fig. 3). The earthquake relocations for 1996–2010 are shown in Figs. 2, 3, and 5 and are listed in Tables 1 and 2. Note that, although the IGUT earthquake catalog begins in 1996, we present the results for two different time intervals (1996–2005 in Table 1; 2006–2010 in Table 2) separately because an upgrade in the network in 2006 caused the earthquake catalog to be revised routinely. The quality and likely accuracy of the arrival-time picks are higher in the time-interval 2006–2010 than 1996–2005. According to the results shown in Fig. 3, the distributions of the horizontal location errors (ERH) and vertical location errors (ERZ) are heavy-tailed and have average of 7.4 and 5.4 km, respectively, and the minor semi-axis and major semi-axis of the corresponding 68 % confidence ellipsoid are 4.7 and 15.1 km, respectively (Fig. 3a and b). With the current seismic station distribution in study area, data gaps are common, particularly for

events outside the seismic network. The location error tends to increase when the azimuthal gap increases (particularly the secondary azimuthal gap), which is typical for a suboptimal sparse network geometry configuration (Fig. 3d and e). The results also indicate a weak correlation between the location error and magnitude (Fig. 3g); however, the location error tends to decrease significantly as the number of associated phases increases (Fig. 3f). Outliers detected by the EDT are depicted in Fig. 3i. The EDT weights presented in Fig. 3i are posterior weights of observed phases which are assigned based on their contributions to the maximum likelihood EDT, as opposed to fixed EDT prior weights. On average, 1.4 outliers were detected per event for well-constrained events, i.e., those with less than 180° azimuthal gap, and a large number of outliers (3.2 cases per event) were observed for those events re-located outside the seismic network with azimuthal gap larger than 180° . In general, EDT weights are

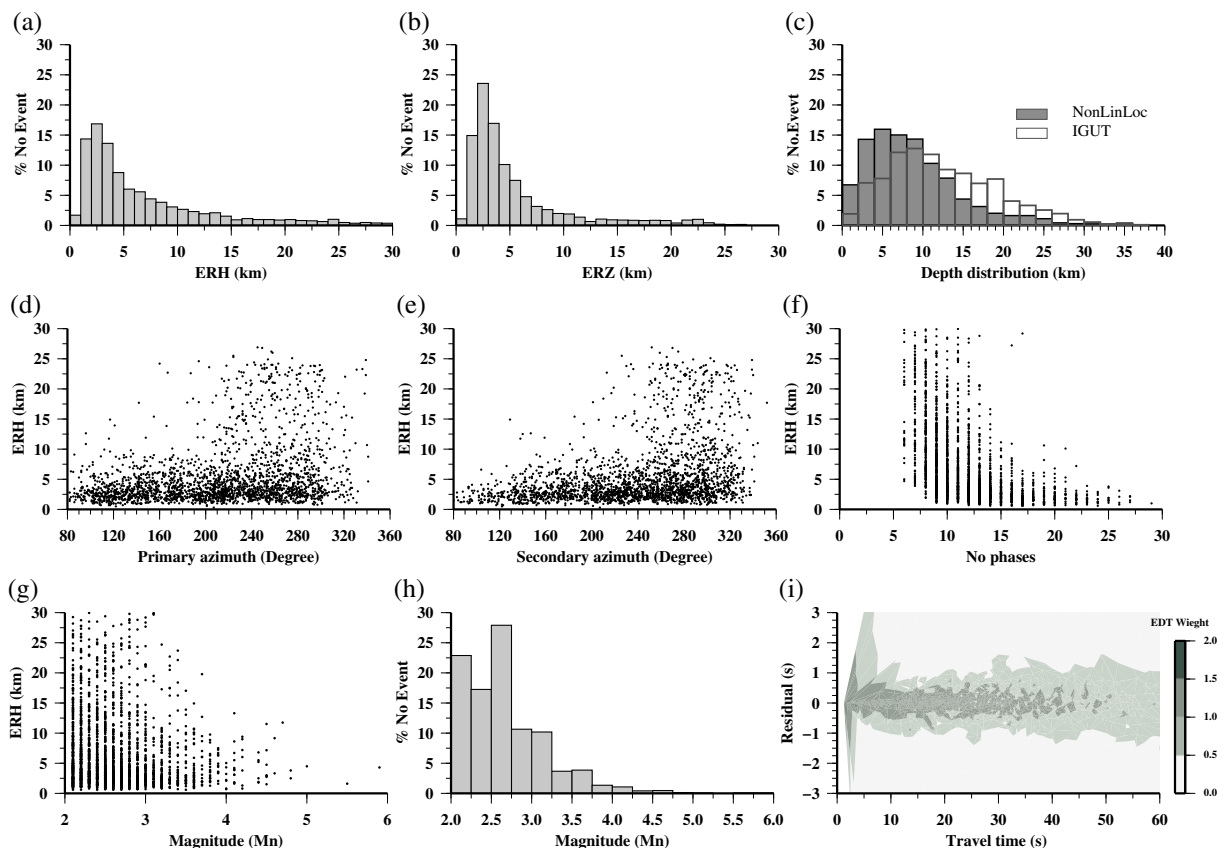


Fig. 3 Results from NLL for solutions with hypocentral errors less than 30 km. Panels **a** and **b** show frequency histograms of the horizontal and vertical errors, respectively. Panel **c** displays the depth distribution histograms. Panels **d–g** show NLL horizontal error as function of **d**

primary and **e** secondary azimuthal gaps, **f** number of P- and S-phases used in the process, **g** magnitude of the events (Mn). Panels **h** and **i** show distribution of earthquake magnitudes and EDT weights applied to different phases

Table 1 The results of relocated earthquake using NLL algorithm for time-interval 1996–2005

Azimuthal gap (°)	ERZ (km)	ERH (km)	No. EQ	Secondary azimuthal gap (°)	ERH (km)	ERZ (km)	Mag. (Mn)	LOGGAU2	No. S	No. P	Distance to closest station	Exp. Location, max. likelihood	RMS NLL (s)
Azimuthal gap < 180	ERZ < 3.0	ERH < 3.0	136	175	1.8	2.1	2.6	0.011	4	13	32.8	1.1	0.25
		ERH > 3.0	51	200	4.8	2.2	2.6	0.012	3	13	27.4	2.3	0.30
	ERZ > 3.0	ERH < 3.0	85	171	2.1	4.2	2.6	0.013	3	12	37.1	3.2	0.24
		ERH > 3.0	235	209	13.5	8.0	2.6	0.026	2	10	32.6	6.4	0.29
Azimuthal gap > 180	ERZ < 3.0	ERH < 3.0	161	254	2.3	2.0	2.6	0.010	5	13	60.7	1.8	0.24
		ERH > 3.0	242	281	5.6	2.2	2.6	0.011	4	12	56.1	2.9	0.32
	ERZ > 3.0	ERH < 3.0	52	245	2.5	3.9	2.6	0.011	4	11	57.1	4.5	0.22
		ERH > 3.0	919	284	15.8	9.8	2.6	0.025	3	10	68.1	9.1	0.36

Parameter LOGGAU2 is a distance weighting used in NLL location algorithm

No. EQ number of earthquakes, Mag magnitude, No. S no. of S phase, No. P no. of P phase

larger at close stations where the travel-times are shorter than distances stations. The residuals for the outliers will be much larger than the average residuals, and the EDT weights will be close to zero for outliers. It makes sense that the EDT weights are lowered with increasing distance when LOGGAU2 is used, since the EDT weights decrease with increasing travel-time error for a fixed residual (see Fig. 3i). EDT weight will in general increase with decreasing residuals, but the maximum weight (at zero residual) is still scaled by the assigned travel-time and picking errors. Low EDT weights and large residuals at travel times of about 5 s may be related to smaller events with fewer picked arrivals and greater sensitivity of the location algorithms to model errors.

A comparison between the locations reported by the IGUT (1996–2010) and the relocations from this study

indicates a total bias of -0.4 km in latitude, 0.7 km in longitude, and -2.7 km in depth in the IGUT catalog (see Fig. 3c). Solutions reported in the IGUT catalog with non-zero depth are typically deeper than the corresponding NLL locations. Note that a systematic shift between two locations can be explained partly by different velocity models used in each case. The earthquake location in the IGUT catalog is based on a simple 1D velocity model (see Fig. 4) over a half-space. However, the error ellipsoids resulting from NLL indicate more reliable solutions even under the ill-conditioned location problem (Fig. 5, Tables 1 and 2). Note that, in Fig. 5, only the NLL solutions with horizontal errors less than 10 km are plotted. The horizontal errors and vertical errors (ERH and ERZ, respectively) are proportional to the root-mean-square of the diagonal elements of the

Table 2 The results of relocated earthquake using NLL algorithm for time-interval 2006–2010

Azimuthal gap (°)	ERZ (km)	ERH (km)	No. EQ	Secondary azimuthal gap (°)	ERH (km)	ERZ (km)	Mag. (Mn)	LOGGAU2	No. S	No. P	Distance to closest station	Exp. Location, max. likelihood	RMS NLL (s)	RMS IGUT (s)
Azimuthal gap < 180	ERZ < 3.0	ERH < 3.0	207	150	1.5	1.8	2.8	0.011	06	11	24.5	0.9	0.29	0.37
		ERH > 3.0	29	177	4.5	2.2	2.5	0.012	04	09	28.9	2.1	0.29	0.33
	ERZ > 3.0	ERH < 3.0	66	159	1.8	3.9	2.6	0.014	04	10	34.8	2.7	0.31	0.33
		ERH > 3.0	64	198	11.2	7.7	2.4	0.032	02	07	33.9	5.9	0.40	0.31
Azimuthal gap > 180	ERZ < 3.0	ERH < 3.0	78	224	2.1	2.0	2.9	0.010	07	11	53.2	1.5	0.30	0.36
		ERH > 3.0	77	248	4.4	2.2	2.9	0.011	05	10	58.2	2.6	0.34	0.35
	ERZ > 3.0	ERH < 3.0	31	230	2.2	3.9	2.7	0.011	05	09	58.9	3.3	0.25	0.36
		ERH > 3.0	257	262	16.7	11.6	2.7	0.030	03	08	76.5	8.6	0.39	0.35

Parameter LOGGAU2 is a distance weighting used in NLL location algorithm

no. EQ number of earthquakes, Mag magnitude, No. S no. of S phase, No. P no. of P phase

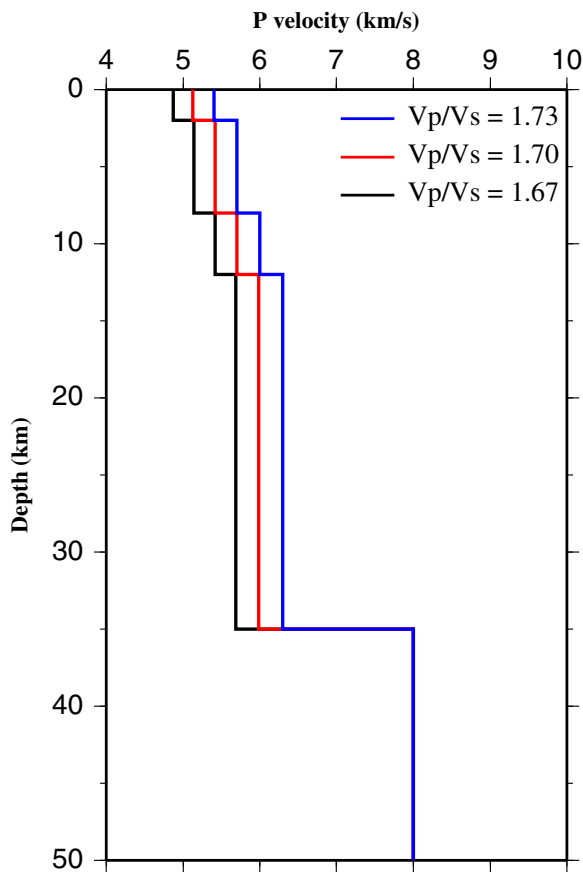


Fig. 4 Different 1D velocity models used in this study and synthetic section. The velocity model developed by Ashtari et al. (2005), 5 % slower than the Ashtari et al. (2005) model and 10 % slower than the Ashtari et al. (2005) model are depicted by blue and red and black colors, respectively

covariance matrix of the errors. In EDT-PDF applications, the corresponding semi-axes for a 68 % confidence ellipsoid (Fig. 5) are related to ERH and ERZ via a chi-squared distribution for a system with three degrees of freedom and a root-mean-square of 3.53. Thus, the semi-axes for a 68 % confidence ellipsoid appear larger than the constraints applied in the relocation process (10 km).

2.1 Cross-sections across the study area

The study area is a complex region of deformation with complicated fault behavior near the surface. Routine IGUT earthquake locations in the region show a diffuse cloud of seismicity distributed over a broad area. Several faults in the Central Alborz region have been mapped at the surface, but their geometries at depth remain unknown. Several cross-sections are

presented here that show earthquakes with horizontal and vertical errors less than 10 km (Figs. 2 and 6). Cross-sections AA' and BB' are taken across the Mosha Fault, one of the most active faults in the Central Alborz region with a high rate of historical seismicity (e.g., Ambraseys and Melville 1982; Berberian 1994; Berberian and Yeats 2001). The relocated earthquakes on the Mosha Fault show a clear north-dipping structure in Fig. 6. Abbassi et al. (2010) detected the same north-dipping structure across the Mosha Fault using a dense temporary seismic network in the study area. The error ellipsoid resulting from the NLL (see Fig. 5) indicates the reliability of the relocated events. Cross-sections across the Garmsar Fault (cross-sections DD' and EE', Figs. 2 and 6) show a more complicated seismicity pattern than the other faults with a component of north dipping structure in cross-section DD' that changes to south-dipping seismicity observed in cross-section EE'. Note that relocated events in cross-sections DD' and EE' are more tightly clustered and align along the dipping structures than the original results. As for the Mosha Fault, the seismicity associated with the Garmsar Fault is limited to the upper 10 km of the crust. The highest seismicity rate in the Tehran region is related to the Mosha and Garmsar faults, which have major north-dipping structures with strong historical earthquakes (e.g., Jackson et al. 2002; Ashtari et al. 2005). The maximum depth of seismicity deepens to the north across the Khazar Fault (cross-sections FF' and GG', Fig. 6), and there are two large clusters of seismicity at shallow depths that show the existence of a south-west dipping fault plane. The seismicity tend to deepen as moving eastward along the Khazar Fault (cross-sections FF' and GG', Fig. 6). Our relocated results indicate that the seismicity along cross-section GG' is concentrated at depth and is not present in the upper 4 km. The same seismicity pattern was also observed by a separate study done by Tatar et al. (2007) using aftershock relocation of the 28 May 2004 Baladeh earthquake (Mw 6.2). Other cross-sections (e.g., cross-section CC' in Fig. 6) show clear south-dipping seismicity without any related surface expressions of faults, which could suggest that faulting occurs deep in the crust and rarely disturbs overlying sediments. Note that the rupture extent of an earthquake is also related to its magnitude, and shallow, small earthquakes are not likely to produce surface rupture.

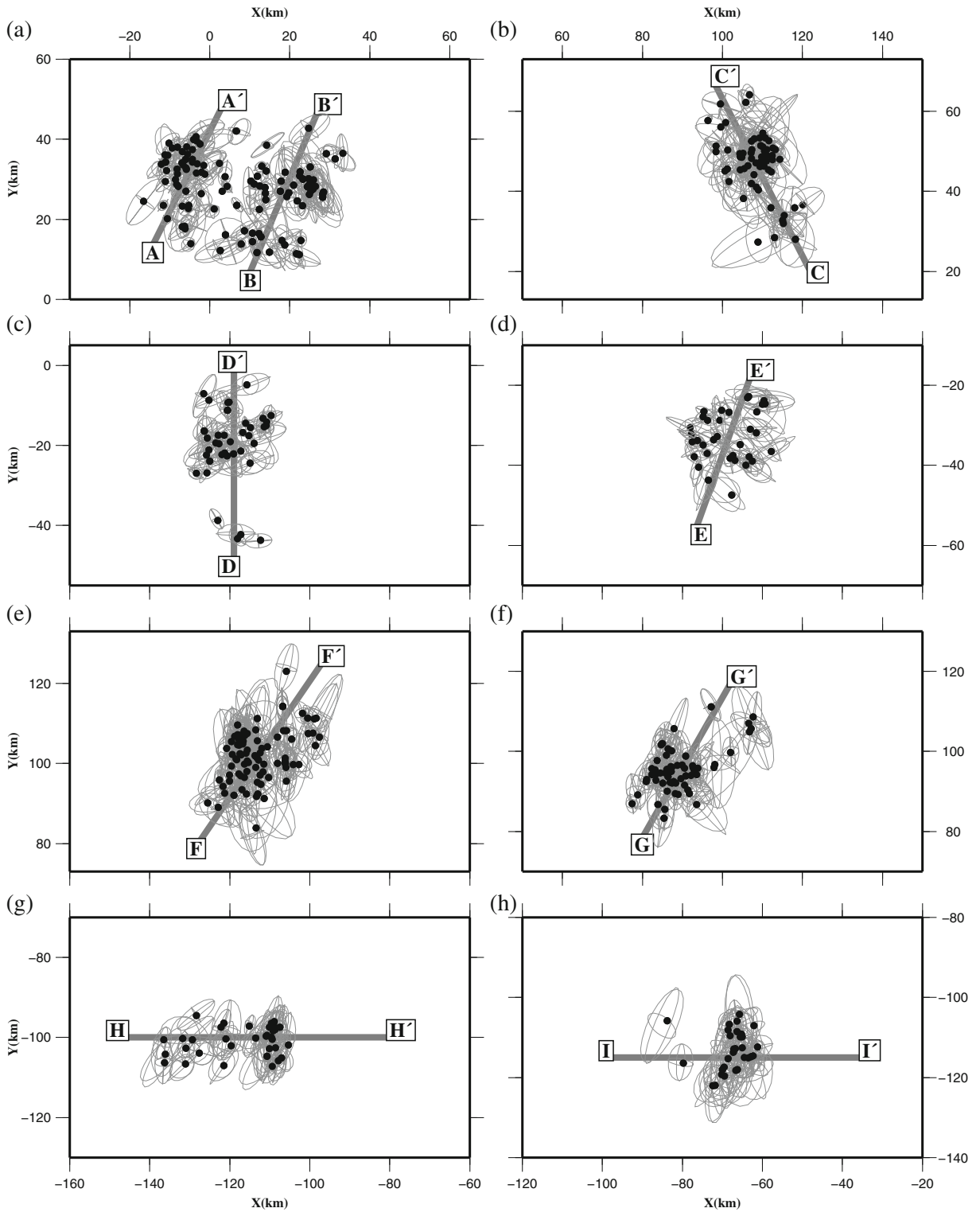
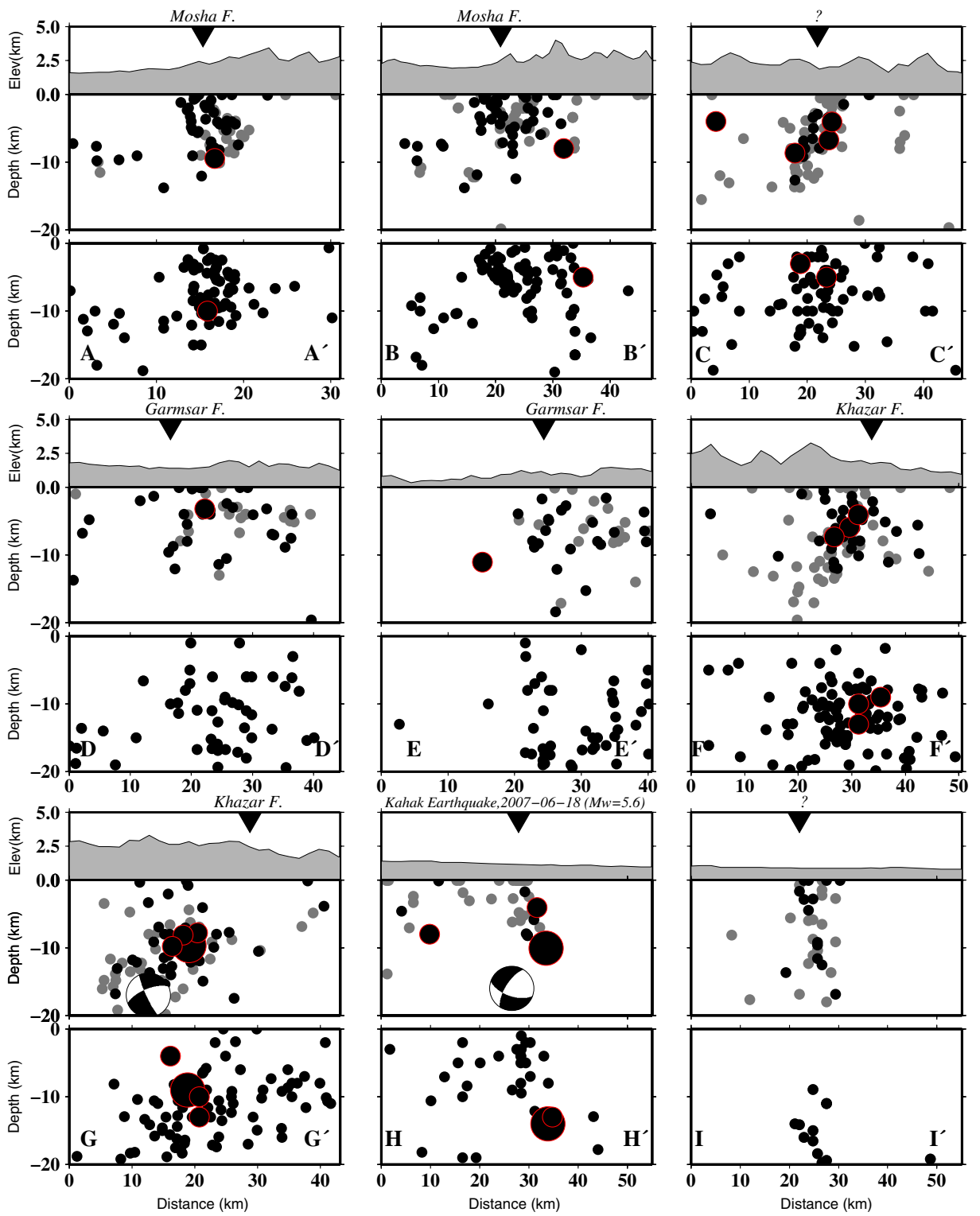


Fig. 5 NLL locations shown as maximum likelihood hypocenters (*black circles*) with 68 % confidence ellipsoids. Only solutions with horizontal errors less than 10 km are shown. Locations of the panels are shown in Fig. 2



◀ **Fig. 6** Vertical cross-sections through relocated data. The cross-section positions are shown in Fig. 2. In each panel, the *upper plot* shows elevation variations along the profile; the *middle plot* shows NLL relocations, and the *bottom plot* shows IGUT catalog seismicity located using hypo71. The cross-sections are 8–15 km wide. The northward dips of the Masha and Garmsar faults can be seen in cross-sections AA' and BB'. The southwestward dipping structure of the Khazar Fault is clear in cross-sections GG' and FF'. The hypocenter of the Mw 5.6 Kahak earthquake, which occurred on 18 June 2007, is shown by the *star* in cross-section H-H'. In panels showing NLL relocations, events with an ERZ less than 3 km are shown in *black*, and those with an ERZ from 3–10 km are shown in *gray*. Fault plane solutions are plotted based on their centroid

2.2 Tests with synthetic data

To investigate the reliability and robustness of the results, various synthetic location scenarios were tested using the same grid spacing, network geometry, and recorded phases as used for the real data (809 events from 2006–2010). Three sets of synthetic tests are presented. In the first test, theoretical and observed arrival times are assumed to have Gaussian uncertainties on the order of 0.01 and 0.05 s for P- and S-phases, respectively, for observational uncertainties and 0.2 and 0.4 s for P- and S-phases, respectively for theoretical uncertainties due to model. These two

types of error have Gaussian distribution and can be modeled by NLL algorithm efficiently. These parameters are used in location to approximate the model error (difference between the model and the true earth). The velocity model developed by Ashtari et al. (2005) with V_p/V_s ratio of 1.73 was employed in the forward and inversion steps in the first test (Figs. 4 and 7, blue curves). Note that the uncertainties assigned for synthetic P- and S-phases are equivalent to typical travel time uncertainties given by parameter LOCGAU2 in the re-location process, which are much larger than the picking uncertainties. In the other two tests, non-Gaussian uncertainties are added to the synthetic data based on assumptions such as error in the forward calculation and a lack of detailed information on the velocity model. In these two synthetic tests, we used the velocity model developed by Ashtari et al. (2005) in the forward travel-time calculation but inverted the synthetic data using slower velocities, i.e., 5 % and 10 % reductions in velocity with V_p/V_s ratios of 1.70 and 1.67 were applied respectively in the second (Figs. 4 and 7, red curves) and third (Figs. 4 and 7, black curves) tests. Location differences (Fig. 7, lower panels) reflect the distance between the original location of the synthetic earthquake and the hypocentral location from NLL. The average differences

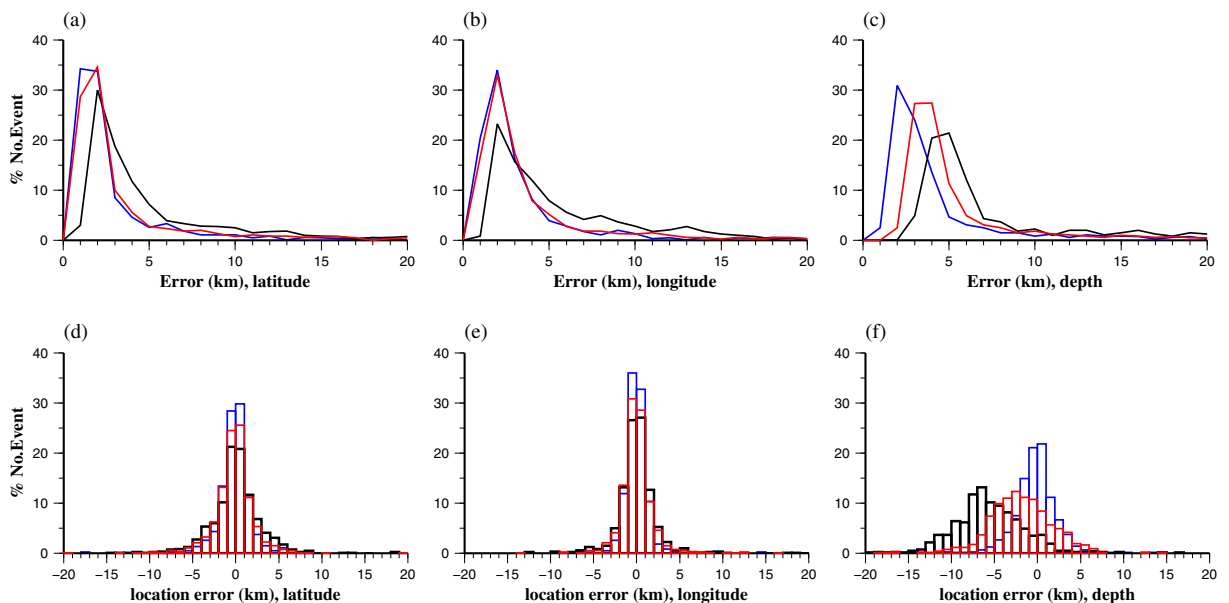


Fig. 7 Synthetic test results. The *upper row* shows hypocentral errors resulting from the NLL algorithm along **a** latitude, **b** longitude, and **c** depth. The *bottom row* shows histograms of the differences between the original locations of the synthetic

earthquakes and relocations (referred to as location error) along **d** latitude, **e** longitude, and **f** depth. *Blue, red, and black curves* are the results calculated based on the different velocity models depicted in Fig. 4

between hypocentral locations obtained by these two different velocity models were about 2.5 and 2.7 km horizontally and 3.9 and 6.5 km vertically for the 5 % and 10 % cases, respectively. Hypocentral location uncertainties resulting from NLL and the location differences in the latitude, longitude, and focal depth (ERX, ERY, and ERZ, respectively) are also shown in Fig. 7. Evaluated location errors in the NLL algorithm are a realistic representation of real error; however, they are mostly slightly larger than the real error. From Fig. 7, the average location errors reported by NLL are about 4.0 and 5.4 km horizontally and 6.1 and 8.3 km vertically, for 5 % and 10 % cases, respectively. These calculations demonstrate that 94 % and 85 % of events contain the true hypocenter locations within 68 % confidence ellipsoid for the 5 % and 10 % cases, respectively. The results show that the location errors produced by the NLL algorithm are larger than the geometric differences between the original and relocated hypocenters, with the differences increasing as the model error increases (not shown). Non-Gaussian uncertainties lead to a significant bias that increase the location error produced by the NLL algorithm compared with the geometric differences. Non-Gaussian uncertainties also cause a shift in depth for the geometric difference distributions, indicating unrealistic depth estimates from using an incorrect velocity model. Our various synthetic tests presented in this article confirm that the location errors of the dataset are both realistic and consistent.

3 Discussion and conclusions

The Central Alborz region has a significant seismic hazard due to large local, although relatively infrequent, earthquakes. This hazard can be addressed using high-resolution relocated earthquakes. The NLL method used in this research has the advantage of simultaneous analysis of large earthquake datasets. The method improves the accuracy of absolute earthquake locations and thus provides a better correlation of event locations to specific active seismogenic structures. Note that the use of a non-linear probabilistic location method only allows to reliably differentiate between well-constrained and poorly constrained hypocenter locations. For well-constrained hypocenter locations, maximum likelihood and expectation hypocenter locations are close, and location uncertainties

are well represented by the 68 % confidence ellipsoid. In absolute terms, a hypocenter location can still be poor if data and seismic models, e.g., 1D velocity model are of poor quality, even if the hypocenter location was computed using a non-linear earthquake location technique. Standard linearized relocation methods for the study region result in a diffuse cloud of seismicity distributed over a broad region, which is mainly due to the ill-conditioned location problem. However, the application of the NLL method leads to clearer and more reliable seismicity patterns and is more effective compared with routinely linearized locations calculated in the IGUT, even under the ill-conditioned problem. Our results show improved definition of active seismogenic sources in the east of the Tehran region associated mainly with known active faults in the study area (the Mosha and the Garmsar faults).

We have relocated 3,012 earthquakes from 1996–2010 that occurred in the Central Alborz region using a non-linear relocation algorithm. The PDFs resulting from this study are significantly compact, providing high-resolution hypocenter locations for the study region. During the re-location process, we observed that, for some events, changes in the depth were accompanied by changes in the epicenter position as observed by Janský et al. (2012). These events showed up as large values in the covariance for XZ and YZ. Also, the ellipsoid and PDF scatter cloud were similar to oblique cylinders, not vertical cylinders. Overall, 816 relocated earthquakes have epicentral uncertainties in the 0.5–3.0 km range, and 981 earthquakes have depth uncertainties less than 3.0 km. Accurate estimates of hypocenter locations and associated uncertainties were used to gain a better understanding of the observed seismicity pattern. After the events were relocated, the majority of the seismicity shows more focused clustering along several known active faults. However, in many circumstances, the seismicity at depth does not correlate with surface faulting, which suggests that the faulting at depth does not offset the overlying sediments directly. Note that the rupture is also related to the magnitude, in the sense that shallow small earthquakes do not necessary make evidence on the surface. After event relocation, the majority of the seismicity occurs in the upper 20 km of the crust, and no deep seismicity (>20 km depth) has been observed, indicating that the thickness of the seismogenic layer in this region is not larger than 20 km. The possibly of future application of relative location methods to some

of the better located clusters of seismicity will be investigated in a separate work.

Acknowledgments Catalog arrival-times were obtained directly from the Iranian Seismological Center, Institute of Geophysics/University of Tehran (<http://irsc.ut.ac.ir/>; last accessed March 2012). The Global Centroid Moment Tensor (CMT) Project catalog was searched using www.globalcmt.org/CMTsearch.html (last accessed March 2012). NLL software, developed by A. Lomax (www.alomax.net/nlloc; last accessed March 2012), was used for as an analyzing tool. Some plots were made using the Generic Mapping Tools (GMT) version 4.2.1 (Wessel and Smith 1998; www.soest.hawaii.edu/gmt, last accessed March 2012). We would like to thank the employees of Iranian Seismological Center, IGUT, especially Saeid Naseri. We also thank Prof. Roland Roberts (Department of Earth Sciences, Uppsala University, Sweden) and Dr. Farzam YaminiFard (International Institute of Earthquake Engineering and Seismology, Iran) for their valuable comments on the manuscript. We would also like to thank the Associate Editor, Professor Jiri Zahradnik and two anonymous reviewers for their constructive comments and useful suggestions.

References

- Abbassi A, Nasrabadi A, Tatar M, YaminiFard F, Abbassi MR, Hatzfeld D, Priestley K (2010) Crustal velocity structure in the southern edge of the Central Alborz (Iran). *J Geodyn* 49:68–78. doi:10.1016/j.jog.2009.09.044
- Allen MB, Ghassemi MR, Sharabi M, Qoraishi M (2003) Accomodation of Late Cenozoic oblique shortening in the Alborz range, northern Iran. *J Struct Geol* 25:659–672
- Ambraseys NN, Melville CP (1982) A history of Persian earthquakes. Cambridge University Press, UK, p 212
- Ashtari M, Hatzfeld D, Kamalian N (2005) Microseismicity in the region of Tehran. *Tectonophysics* 395:193–208. doi:10.1016/j.tecto.2004.09.011
- Berberian M (1994) Natural hazards and the first earthquake catalogue of Iran. Volume 1: historical hazards in Iran prior to 1900. *Int. Inst. Earth-quake Engineering and Seismology*, Tehran.
- Berberian M, (1976) Contribution to the seismotectonics of Iran (Part II). pp. 518, Report No. 39, Geological Survey of Iran, Iran.
- Berberian M, Yeats RS (1999) Patterns of historical earthquakes rupture in the Iranian plateau. *Bull Seism Soc Am* 89:120–139
- Berberian M, Yeats RS (2001) Contribution of archaeological data to studies of earthquake history in the Iranian plateau. *J Struct Geol* 23:563–584
- Font Y, Kao H, Lallemand S, Liu CS, Chiao LY (2004) Hypocentre determination offshore of eastern Taiwan using the maximum intersection method. *Geophys J Int* 158 (2):655–675
- Husen S, Kissling E, Deichmann N, Wiemer S, Giardini D, Baer M (2003) Probabilistic earthquake location in complex three-dimensional velocity models: application to Switzerland. *J Geophys Res* 108(B2):2077
- Husen E, Smith RB (2004) Three-dimensional velocity models for the Yellowstone National Park Region, Wyoming. *Bull Seismo Soc Am* 94:880–895
- Jackson J, Priestley K, Allen M, Berberian M (2002) Active tectonics of the South Caspian Basin. *Geophys J Int* 148:214–242
- Janský J, Novotný O, Plicka V, Zahradník J, Sokos E (2012) Earthquake location from P-arrival times only: problems and some solutions. *Stud Geophys Geod* 56:553–566. doi:10.1007/s11200-011-9036-2
- Lahr JC (1989) HYPOELLIPSE/version 2.0:a computer program for de-tecting local earthquake hypocentral parameters, magnitude, and first motion patterns. U.S. Geological Survey Open File Report. 8–116.
- Lawson CL, Hanson RJ (1974) Solving least squares problems. Prentice Hall, Englewood Clifts, NJ
- Lee WHK, Stewart SW (1981) Principles and applications of microearthquake networks. Academic Press, New York, p 293
- Lomax A (2005) A reanalysis of the hypocentral location and related observations for the Great 1906 California Earthquake. *Bull Seismol Soc Am* 95:861–877
- Lomax A, Cattaneo M, Bethoux N, Deschamps A, Courboux F, Déverchère J, Virieux J (1998) Comparison of linear and non-linear earthquake locations for the 1995 Ventimiglia sequence. Poster presentation at: European Geophysical Society, XXII General Assembly, <http://alomax.free.fr/posters/vintimiglia>.
- Lomax A, Curtis A (2001) Fast, probabilistic earthquake location in 3D models using Oct-Tree Importance sampling. *Geophys. Res. Abstr.*, 3.
- Lomax A, Michelini A, Curtis A (2009) Earthquake location, direct, global-search methods. In: Meyers RA (ed) Complexity in encyclopedia of complexity and system science, part 5. Springer, New York, pp 2449–2473. doi:10.1007/978-0-387-30440-3
- Lomax A, Virieux J, Volant P, Berge C (2000) Probabilistic earthquake location in 3D & layered models: introduction of a Metropolis-Gibbs method & comparison with linear locations. In: Thurber CH, Rabinowitz N (eds) Advances in seismic event location. Kluwer, Amsterdam, pp 101–134
- Lomax A, Zollo A, Capuano P, Virieux J (2001) Precise, absolute earthquake location under Somma-Vesuvius volcano using a new 3D velocity model. *Geophys J Int* 146:313–331
- Moinfar A, Mahdavian A, Maleki E (1994) Historical and instrumental earthquake data collection of Iran. Publication Iranian Culture. Affairs Inst, Tehran, p 446
- Van Moser TJ, Eck T (1992) Hypocenter determination in strongly heterogeneous earth models using the shortest path method. *J Geophys Res* 97:6563–6572
- Nuttli OW (1973) Seismic wave attenuation relations for eastern North America. *J Geophys Res* 78:876–885
- Presti D, Orecchio B, Falcone G, Neri G (2008) Linear versus non-linear earthquake location and seismogenic fault detection in the southern Tyrrhenian Sea, Italy. *Geophys J Int* 172:607–618
- Presti D, Troise C, De Natale G (2004) Probabilistic location of seismic sequences in heterogeneous media. *Bull seism Soc Am* 94(6):2239–2253

- Satriano C, Lomax A, Zollo A (2008) Real-time evolutionary earthquake location for seismic early warning. *Bull Seismol Soc Am* 98:1482–1494
- Tarantola A, Valette B (1982) Inverse problems=quest for information. *J Geophys* 50:159–170
- Tatar M, Jackson J, Hatzfeld D, Bergman E (2007) The 2004 May 28 Baladeh earthquake (M_w 6.2) in the Alborz, Iran: overthrusting the South Caspian Basin margin, partitioning of oblique convergence and the seismic hazard of Tehran. *Geophysical J Int*, 170: 249–261. doi: [10.1111/j.1365-246X.2007.03386.x](https://doi.org/10.1111/j.1365-246X.2007.03386.x)
- Vernant P, Nilforoushan F, Chéry J, Bayera R, Djamour Y, Masson F, Nankali H, Ritz JF, Sedighi M, Tavakoli F (2004) Deciphering oblique shortening of central Alborz in Iran using geodetic data. *Earth Planet Sci Lett* 223:177–185
- Wessel P, Smith WHF (1998) New, improved version of generic mapping tools released. *Eos Trans Am geophys Un* 79:579